Modelagem Matemática e Investigação Experimental da Evolução das Tensões na Soldagem de Aço

Mathematical modeling and experimental investigation of the stress evolution at the steel welding

Horácio Guimarães Delgado Junior[1]
Carlos Roberto Xavier[2]
José Adilson de Castro[3]
Marcos Flávio Campos[3]
Alexandre Alvarenga Palmeira[1]
Alexandre Fernandes Habibe[1]

Palavra chave:

Soldagem

Modelamento matemático

Distribuição de temperatura

Análise de tensões

Plasticidade

Resumo:
O objetivo deste trabalho é estudar por análise dilatométrica à sinterização após a soldagem dos aços é comum observar deformações das quais podem ser associadas a estados de tensões independentemente do processo utilizado. Este artigo apresenta os resultados da evolução das tensões durante a soldagem de aços obtidos pelo método dos volumes finitos com a implementação do modelo transiente termo-mecânico-metalúrgico com a consideração da interdependência entre as propriedades geométricas, física e metalúrgica. O modelo inclui variações do módulo de elasticidade, do limite de elasticidade ambos dependendo da temperatura e ainda das transformações de fase. Para a distribuição do calor na região da solda foi utilizado o modelo de Goldak. A tensão efetiva é calculada pelo critério de escoamento de Von Mises. Os resultados experimentais das tensões residuais foram analisados através do ruído Barkhausen e as medições de deformação residual foram obtidos por meio do ASAME.

Abstract:
After the welding of the steels is common to observe some kind of deformation and stress states may be consequently associated independently of the process used. This paper presents the results of the evolution of stresses during the welding of steels obtained by the finite volume method by implementing the transient thermo-mechanical-metallurgical model where its geometric properties are physical and metallurgical dependent. The model includes changes of the elastic modulus and yield stress with temperature and the phase transformations. The Goldak's double ellipsoid model for welding heat distribution was used to calculate the distribution of volumetric density of heat flow at the weld pool vicinity. The effective stress is calculated by the Von Mises yield criterion. The experimentals results of the residual stress and metallurgical transformation were analyzed by the Barkhausen noise and the residual strain measurements were obtained by the ASAME (automated strain analysis and measurement environment)

Keywords:

Welding;

Numerical Predictions;

Temperature distribution;

Stress analysis;

Plasticity;

[1] UniFOA e Universidade do Estado Rio de Janeiro

[2] Petrobras e UniFOA

[3] Universidade Federal Fluminense-Polo Universitário de Volta Redonda

Cadernos UniFOA
Edição Especial do Curso de Mestrado Profissional em Materiais - Junho/2013

1. Introduction

Welding process applies to several process of fabrication of metallic structures, ships, pipelines, spaceships, nuclear reactors, and pressure vessels. However, a common problem associated with welding is the residual stresses and permanent deformations introduced in this procedure. The highly localized transient temperature field in the welding processes causes non uniform thermal expansion and contraction, resulting in residual stresses and distortion in the welded structures. High-tensile residual stresses in regions near the weld may promote brittle fracture, fatigue and stress corrosion cracking. Therefore, control and accurate evaluation of weld residual stresses and distortion is an important task in welding manufacturing. Some experimental techniques are used in order to measure residual stresses from metals welding such as hole drilling and x-ray methods. However, some experimental methods disadvantages can be mentioned such as elevated costs requiring special equipment and trained personnel for its application beyond the fact that to obtain a complete map of residual stresses distribution in a typical application is practically impossible in such a way. Therefore, due to the complexity involved in the measurement of residual stresses, there has been an increasing use of numerical simulation procedures for estimating the residual stresses during welding. In this work, a coupled thermostructural 3D model that apply the finite volume method and the adaptive meshes technique for the addition of filler material in the weld pool was developed and implemented in a computational code based on FORTRAN programming language aiming the analysis of stresses evolution during the steel welding.

2. Welding Modeling

2.1. Thermo-Elasto-Plastic Modeling (Tep)

The behaviour of TEP[3] material is governed by the following conservation equations:

• Equation of thermal energy balance,

$$\frac{\partial}{\partial t}\left(\rho c_p T\right)+div\left[\rho c_p\left(\vec{v}\right)T\right]=div\left[k\left(grad\left(T\right)\right)\right]+S \quad (1)$$

• Equation of momentum balance of Cauchy's first law of motion,

$$\frac{\partial}{\partial t}\left(\rho\frac{\partial u_i}{\partial t}\right)+div\left[\rho v u_i\right]=\frac{\partial \sigma_{ij}}{\partial x_j}+f_i \quad (2)$$

• Equation of moment of momentum balance or Cauchy's second law of motion,

$$\sigma_{ij}=\sigma_{ji} \quad (3)$$

In the above equations, t is time, x_j Cartesian spatial coordinates, $\vec{v}$ velocity, ρ density, c_p specific heat, T temperature, q_j heat flux, u_i displacement, σ_{ij} stress tensor, S_T heat source and f_i body force.

Constitutive Relations

Equations (l)-(3) make an open system consisting of 7 equations with 16 unknowns (T, u_i, q_j, σ_j). In order to close that system, the following constitutive relations are used:

• Fourier law, which links the heat flux with spatial gradient of temperature, included in equation (1).

$$q_j=k\frac{\partial T}{\partial x_j} \quad (4)$$

where k is thermal conductivity and

• the relation between the TEP stresses and strains

$$d\sigma_{ij} = 2\mu d\varepsilon_{ij} + \lambda\delta_{ij} d\varepsilon_{kk} - (3\lambda + 2\mu)\alpha\delta_{ij}(T - T_r) - \left\{ \frac{3G\sigma_{ij}^{d}\sigma_{kl}^{d} d\varepsilon_{kl}}{\bar{\sigma}^{2}\left(\frac{H'}{3G} + 1\right)} \right\} \tag{5}$$

where

$$\varepsilon_{ij} = \frac{1}{2}\left(\frac{\partial u_i}{\partial x_j} + \frac{\partial u_j}{\partial x_i} \right) \tag{6}$$

is the strain tensor,

$$\sigma_{ij}^{d} = \sigma_{ij} - \frac{1}{3}\delta_{ij}\sigma_{kk} \tag{7}$$

is the deviator stress tensor,

$$\bar{\sigma} = \left(\frac{3}{2}\sigma_{ij}^{d}\sigma_{ij}^{d} \right)^{\frac{1}{2}} \tag{8}$$

is the effective stress (in the case of Von Mises yield criterion), μ and λ are Lame's constants, (α is the thermal expansion coefficient, G = μ shear modulus, H' is the plastic modulus, T, is the reference temperature, which corresponds to a thermally undeformed state, and δ_{ij} Tis the Kronecker delta. Lame's constants are related to the more commonly used elastic modulus ***E*** and Poisson's ratio *v* by the following relationships:

$$\lambda = \frac{\nu E}{(1+\nu)(1-2\nu)} \qquad \mu = G = \frac{E}{\nu(1+\nu)} \tag{9}$$

In the case of elastic conditions, the expression within the brackets { } vanishes, and the constitutive relation (5) reduces to the Duhamel-Neumann form of Hooke's law.

Mathematical Model

By combining (l)-(5), the following equations can be obtained:

$$\frac{\partial}{\partial t}\left(\rho c_p T\right) + div\left[\rho c_p\left(\vec{v}\right)T\right] = div\left[k\left(grad\,(T)\right)\right] + S \tag{10}$$

$$\frac{\partial}{\partial t}\left(\rho\frac{\partial \delta u_i}{\partial t} \right) + div\left[\rho c_p\left(\vec{v}\right)\frac{\partial \delta u_i}{\partial t} \right] = \frac{\partial}{\partial x_j}\left(\mu\frac{\partial \delta u_i}{\partial x_j} \right) + \frac{\partial}{\partial x_j}\left(\mu\frac{\partial \delta u_j}{\partial x_i} \right) + \frac{\partial}{\partial x_i}\left(\mu\frac{\partial \delta u_k}{\partial x_k} \right) \tag{11}$$

where δT and δu_i are temperature and displacement increments, respectively. These equations make a closed system of four equations with four unknowns (δT, δu_i). Since the material physical properties (*c, k, μ, λ, α*) are in general functions of temperature, the equations (10) are non-linear and coupled, even in the thermo-elastic case. In the case where the part of the heat energy source term coming from the thermo-elastic cooling/ heating due to the elastic volume change $(3\lambda + 2\mu)\alpha T_r(\partial\varepsilon_k/\partial t)$ can be neglected $(1/3\alpha)(\partial\varepsilon_k/\partial t)$ $(\partial T/\partial t)$, the heat energy equation is decoupled from the momentum equations and can be solved independently. However, in order to solve momentum equations, the temperature field has to be known. In order to complete a mathematical model, initial and boundary conditions are to be provided. The initial condition temperature and displacements in the whole solution domain at the initial instant of time have to be given. Boundary conditions can be either of Dirichlet or Von Neuman type, i.e. temperature and/or heat flux and displacements and /or forces (surface tractions) have to be specified at all boundaries.

2.2. Thermal Boundary Condition

a) The energy added to the plate was calculated by the product of current through the welding voltage obtained from the experimental procedure. The Goldak's double ellipsoid model for welding heat distribution was used

to calculate the distribution of volumetric density of heat flow at the weld pool vicinity.

b) We adopted a global coefficient for the entire board, which involved the loss of heat by convection and radiation, whose estimated value was 150 W/m2K.

2.3. Initial Condition

a) Temperature: 25ºC on all sides of the plate;

b) Concentration: corresponding to the chemical composition of steel.

2.4. Modeling the Kinetics of Phase Transformation

In this work we used an extended model of Avrami kinetic law proposed by Reti et al. [8] in order to predict the formation of ferrite, pearlite and bainite during continuous cooling after austenitizing steel hipoeutetóides low-alloy,

$$\frac{dy_i}{dt} = (1 - y_1 - y_2, ..., y_n)\frac{dB_i t^m}{dt} \quad i = 1, 2, ..., n \quad (12)$$

where

- $y_1, y_2, ..., y_n$ Match the volume fraction of phases;
- m Is the Avrami coefficient;
- $B_i = B_i(T)$ Are parameters characterizing the rates of nucleation and growth processes (obtained from the TTT curves) which are redefined to take into account also the effect of austenite grain size in the transformations. Already the formation of martensite was regarded as dependent solely on temperature, according to the Koistinen-Marburger equation [6]

$$f = 1 - \exp\left(-0,011\left(M_s - T\right)\right) \; T \leq M_s \quad (13)$$

which f corresponds to the volume fraction of martensite formed and corresponds to the temperature at the beginning of its transformation (obtained from the TTT curve).

2.5. Numerical Solution

The numerical simulation was based on the finite volume method using the technique of adaptive meshes with the purpose of tracking the formation of the weld bead. The finite volume method was adapted to a system of generalized coordinates (not orthogonal), which allowed to represent accurately the final geometry of the welded plate. The solution of the discretized equations was obtained through line by line method described in Patankar [1] and based on the tri-diagonal algorithm. The solution of the equations was performed in a coupled way represent the interactions of temperature fields and phase transformation in addition to considering the nonlinearities of the properties of steels as a function of temperature and phases present.

3. Results

3.1. Numerical Results

The Figure (1) present the overview of the finite volume mesh used for simulated.

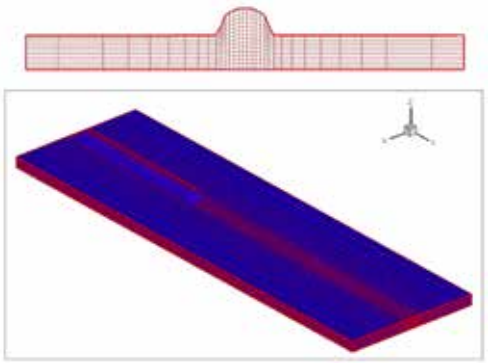

Figure 1. Finite volume mesh.

Toward X specimen has 60 mm wide and were divided into 32 volumes of varying sizes being more refined in the vicinity of the weld bead - the region of greatest interest. Toward Y body of evidence has 200 mm in length were divided into 100 volumes of equal size. Finally toward Z body of evidence has 5.0 mm thick which were divided into 17 equal volumes.

This chapter will present the results expressed in units of the international system (SI), obtained from numerical simulation for the evolution of temperature, stress (S) and their respective components additive thermal (STH), elastic (SE) and plastic (SP), equivalent Von Misses (SigmaBarra) and the values of the deformations (E).

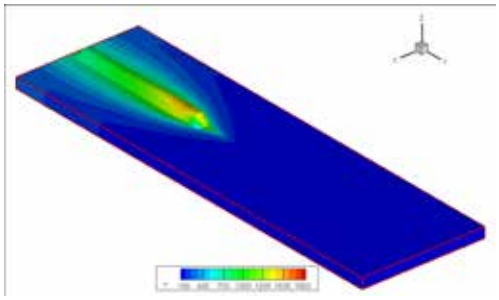

Figure 2. Distribution of Temperature for Steel AISI 4340 after 15s.

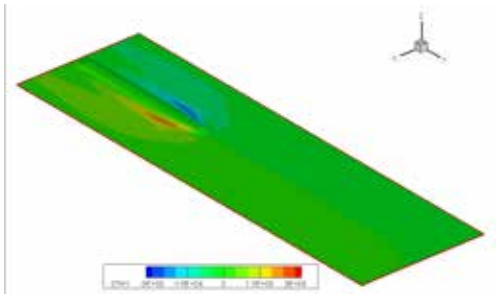

Figure 3. Section STH1 for AISI 4340 Steel after 15s.

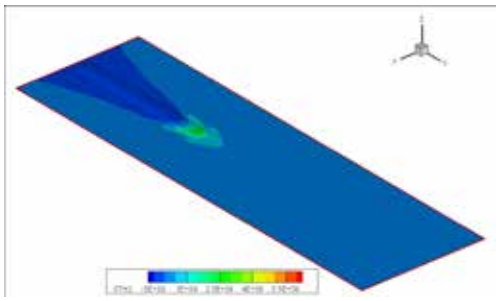

Figure 4. Section STH2 for AISI 4340 Steel after 15s.

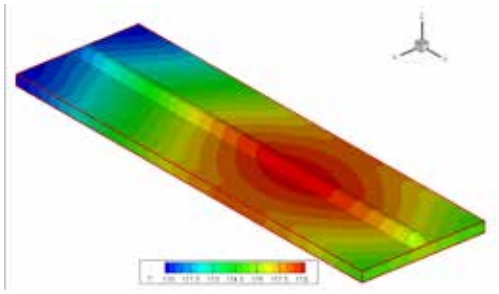

Figure 5. Distribution of Temperature for Steel AISI 1020 after 450s.

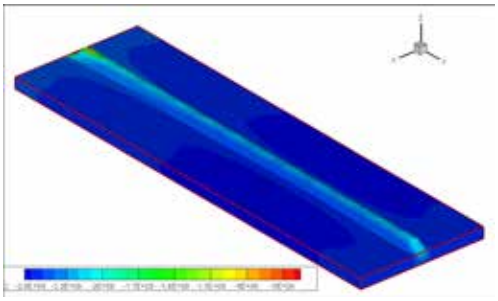

Figure 6. S22 for the steel AISI 1020 after 450s.

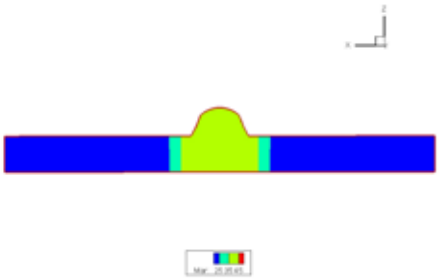

Figure 7. Numerical simulation results for the steel AISI 4340 after welding: martensite.

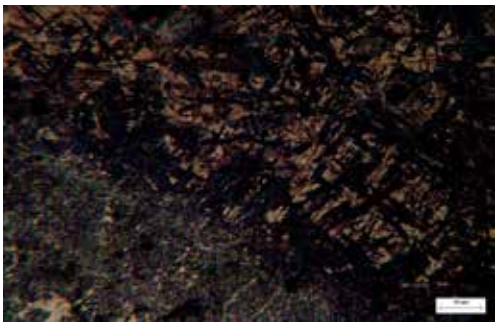

Figure 8. micrograph for the steel AISI 4340 after welding: martensite (200x)

4. Experimental Results

Table 1 shows the chemical composition of steels tested.

Table 1. Chemical analysis of steel (weight %).

AÇO	C	Mn	P	S	Si	Cr	Ni	Mo
AISI-4340	0,39	0,69	0,015	0,011	0,26	0,78	2,08	0,25
AISI-1020	0,19	0,70	0,013	0,012	0,28	-	-	-

This section will present the results of hysteresis curves and analysis of the envelope Barkhausen[4].

Cadernos UniFOA
Edição Especial do Curso de Mestrado Profissional em Materiais - Junho/2013

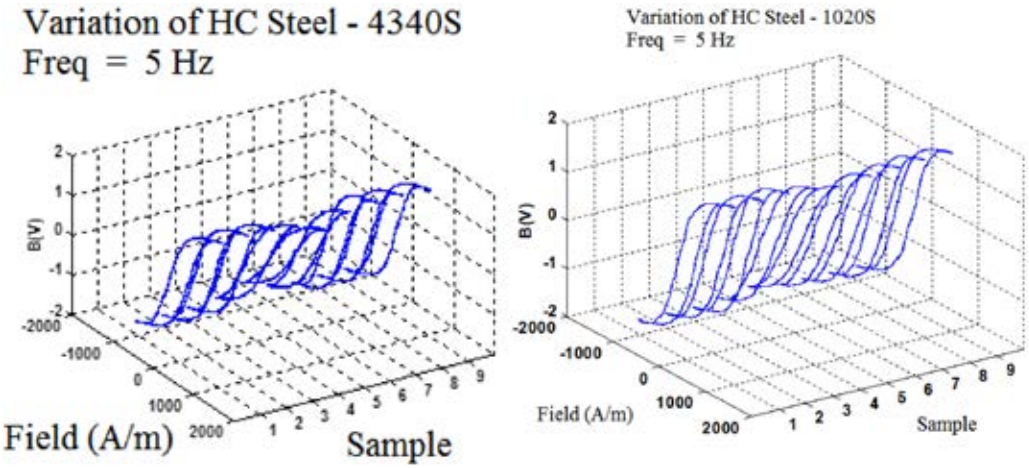

Figure 9. Barkhausen: transverse hysteresis after welding for steels AISI4340 and AISI1020.

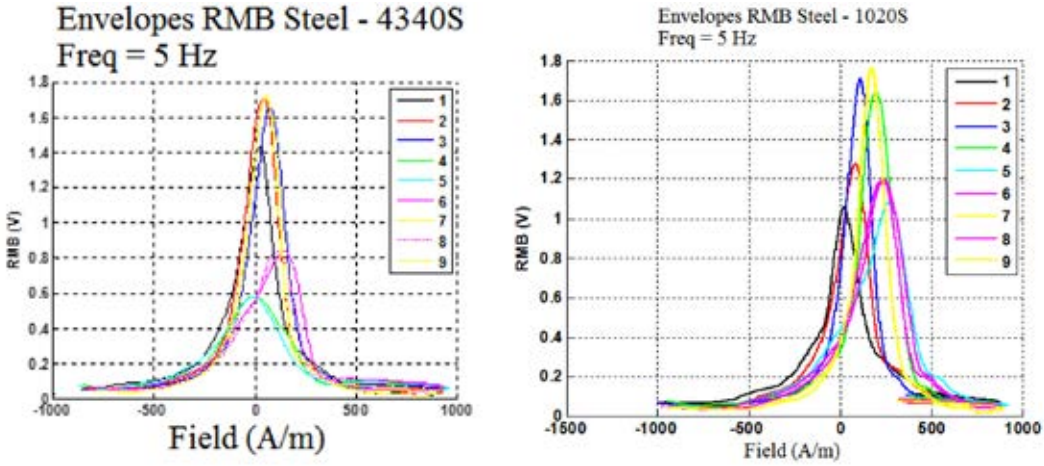

Figure 10. Barkhausen envelope after welding for steels AISI4340 and AISI 1020.

Comparing the deformations measured in the ASAME and the numerically simulated after welding can be observed that the residual strains are very small. The deformations in the ASAME measures are limited to precision tool for marking the grid.

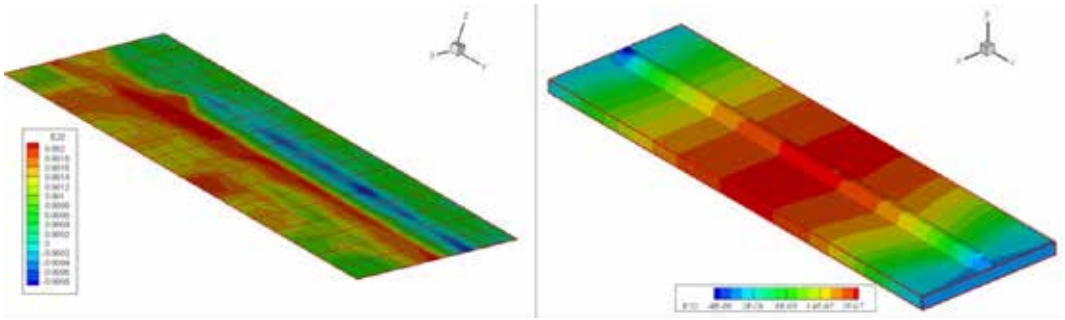

Figure 11. Deformation E22 after welding measures with the ASAME and numerical simulate.

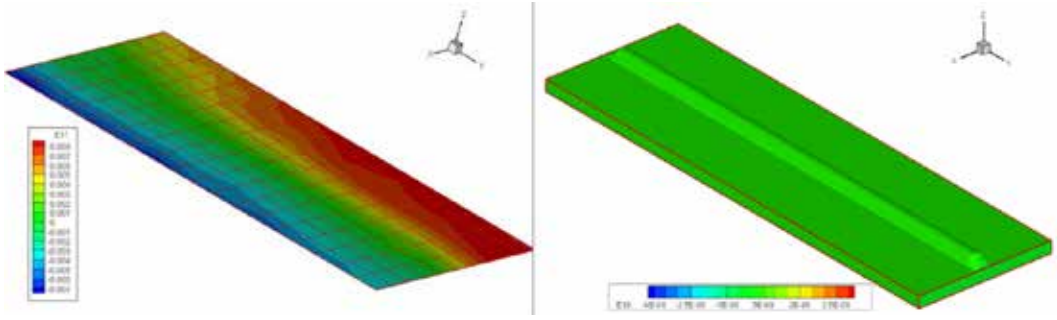

Figure 12. Deformation E11 after welding measures with the ASAME and numerical simulate.

5. Conclusions

1 - The proposed model shows good agreement with experimental results, allowing to predict how the stress state during the welding process of steel since the beginning of the deposition of filler metal to the final cooling.

2 - Comparing the simulation results for the AISI 4340 and AISI 1020 is observed that the phase transformation did not influence the values of the stresses and deformations.

3 - The temperature gradient caused by the deposition of filler metal is who most influences the deformation gradients and consequently the evolution of stress fields and deformations. Certainly hence the appearance of residual stresses in the region of onset of cooling after welding.

4 - The results indicate that the welding process can be analyzed by means of Barkhausen signals. The most significant changes occurred for the display of AISI 4340 steel, which is a high hardenability. Therefore, this material is expected in the region of the weld (HAZ) a larger amount of martensite in carbon steel, as revealed by the simulation.

5 - If the carbon steel AISI1020, changes in both the hysteresis curve as the envelope of the Barkhausen signal can be more directly attributed to residual stresses.

6 - The conclusion is that the analyzing Barkhausen and hysteresis curves reflect the microstructural changes and changes in residual stresses that occurred in the welding process, and that these techniques are useful for pointing out the difference in the process of welding of different materials, in this case, carbon steel and AISI1020 AISI4340.

7 - The results indicate that, because it is difficult to separate the effects due to microstructural phase changes (martensite formation) of the effects of residual stresses proper, the method barkhaseun is primarily a tool for qualitative analysis, and analyzed for the case use of the model provides a quantitative prediction.

8 - In the cases tested computationally and experimentally the residual strains observed were very small.

9 - Comparing the residual stresses obtained by numerical methods with those obtained from the analysis barkhaseun both show the same qualitative interpretation.

6. Acknowledgements

Professor R. Linilson Padovese, Associate Professor of Mechanical Engineering Department of USP and Dr. Freddy E. Franco, for their support in carrying out measures magnetic Barkhausen.

7. References

[1] S. V. Patankar, *Numerical Heat Transfer and Fluid Flow*, McGraw-Hill, New York, (1984), 90.

[2] K.C. Karki and S. V. Patankar: *Numerical Heat Transfer*, **14** (1988), 295.

[3] Demirdzic, I. and Martinovic, D., *Finite volume method for thermo-elasto-plastic stress analysis*, Computer Methods in Applied Mechanics and Engineering, 109, 331-349, North-Holland (1993)

[4] BARKHAUSEN, H.,*Two with help of new repeating rediscovered appearances by H Barkhausen* - The silence during unmagnetising of iron. Physikalische Zeitschrift, v. 20, p. 401-403, 1919.

[5] GOLDAK J.; CHAKRAVARTI, A.; BIBBY, *M. A New Finite Element Model for Welding Heat Sources Model*. Metallurgical Transactions B, v. 15B, p. 299-305, Jun. 1984.

[6] PATANKAR, S. V. *Numerical Heat Transfer and Fluid Flow*. McGraw-Hill. USA, 1979.

[7] MELAAEN, M. C. *Calculation of Fluid Flows with Staggered and Nonstaggered Curvilinear Nonortogonal Grids* – The Theory. Numerical Heat Transfer, Part B, v. 21, p. 1-19, 1992.

[8] RETI, T., FRIED, Z., FELDE, I., *Computer Simulation of Steel Quenching Process Using a Multi-Phase Transformation Model***,** Computational Materials Science, Vol.22, 2001, p. 261-278.